JOURNAL OF GEOPHYSICAL RESEARCH, VOL. 90, NO. C6, PAGES 11,959–11,966, NOVEMBER 20, 1985

Internal Wave Dissipation Under Sea Ice

JAMES H. MORISON

Polar Science Center, University of Washington, Seattle

CHARLES E. LONG

Research Division, Coastal Engineering Research Center, U.S. Army Engineer Waterways Experiment Station, Vicksburg, Mississippi

MURRAY D. LEVINE

College of Oceanography, Oregon State University, Corvallis

The dissipation of internal wave energy in the turbulent boundary layer under pack ice is determined using a time-varying boundary layer model with an eddy coefficient closure scheme. The magnitude of the eddy coefficient is determined by the ice drift velocity, which is assumed greater than the rms water velocity induced by internal waves. The Arctic Ocean internal wave velocity spectrum is represented by a line spectrum with 44 rotary frequency components. The energy at a given frequency is set equal to the energy in a band about the frequency in the continuous spectrum. The dissipation spectrum is found to have an ω^{-2} shape. For an internal wave energy level representative of Arctic Ocean conditions (energy parameter r equal to 50 m^2 cph) the total dissipation is 0.16 mW m^{-2}. This corresponds to a dissipation time scale of 32 days and suggests that underice dissipation is important. The surface boundary layer dissipation process is unique to ice-covered regions, and the predicted amount of dissipation appears to be great enough to explain earlier observations that the internal wave energies in the Arctic Ocean are low compared to internal wave energies measured in ice-free oceans.

1. INTRODUCTION

Despite the intensive study of oceanic internal waves over the past several decades by both experimentalists and theoreticians there are significant deficiencies in our understanding of the physical processes that generate, modify, and dissipate internal waves (see recent reviews by *Munk* [1981], *Olbers* [1983], and *Levine* [1983]). On the basis of a set of diverse field evidence, *Garrett and Munk* [1972, 1975, 1979] (hereafter referred to as GM) presented the surprising result that the internal wave spectrum is remarkably constant in time and space. Subsequent experiments have generally confirmed the GM hypothesis. As a means of identifying possible sources and sinks of internal waves, *Wunsch* [1976] suggested searching for geographical regions where the internal wave field deviated from the canonical GM spectrum. The Arctic Ocean appears to be one location where deviations do exist. Preliminary studies suggest that the internal wave energy under the Arctic ice cover is lower than usually observed in temperate oceans [*Morison*, 1985; *Levine et al.*, 1985]. *Morison* [1985] has examined historical data from *Yearsley* [1966], *Neshyba et al.* [1972], *Bernstein and Hunkins* [1971], and *Bernstein* [1971] and has found that while the forms of the internal wave spectra from the Arctic are of the same shape as the GM model, the energy levels are 0.05 to 0.33 times lower. Recent data gathered in the Arctic by *Levine et al.* [1985] also show low energy levels, from 4 to 6 times lower than the canonical values.

There are several possible explanations for this reduced energy level. The forcing of internal waves in the Arctic may be substantially less than at lower latitudes. The ice cover eliminates most surface wave forcing. Also, tides are generally weak in the Arctic, and above 75°N the tidal frequencies lie outside the internal wave frequency band. However, these reductions may be offset by forcing that is unique to the Arctic, such as the motion of pressure ridge keels on the underside of the ice and the strong buoyancy flux that occurs in leads.

The internal wave energy may also be less in ice-covered waters because of increased energy dissipation, and that is the subject of this paper. Figure 1 illustrates how dissipation is enhanced by a surface ice cover. The ice pack provides a lid that is effectively rigid for most internal wave frequencies and horizontal wavelengths. Thus, unlike the waves in an ice-free ocean, the waves under ice must generate oscillatory boundary layers at the surface. These are embedded in and interact with the turbulent boundary layer that exists without the waves. Such oscillating boundary layers may provide an important sink for internal wave energy, one which does not exist in the open ocean. *D'Asaro* [1982] discusses the absorption of internal wave energy in the bottom boundary layer and estimates that the absorption ranges from -0.003 to 0.024 mW m^{-2}. This indicates bottom absorption is unimportant. However, for typical profiles of the Brunt-Vaisala frequency N, the internal wave modal structure yields much higher horizontal velocities near the surface than at the bottom. Thus dissipation may be much larger in a surface boundary layer than in a bottom boundary layer for the same level of internal wave energy per unit area. The problem of internal wave dissipation under ice has been addressed for a special case by *Levkov and Cherkesov* [1974]. They discuss the behavior of long surface and interfacial waves in an ice-covered, viscous, two-layer ocean forced by a fluctuating surface pressure. The ice cover damps the interfacial waves substantially, by a factor of $2 + (\nu_1/\nu_2)^{1/2}$ over the no–ice cover case, where ν_1 and ν_2 are upper and lower layer viscosities.

In this paper we estimate the energy dissipation using a model of oscillating boundary layers developed by *Long* [1981]. The model employs an eddy coefficient and is solved numerically. The eddy coefficient requires specification of single-velocity and single-length scales and is based on the

Paper number 5C0435.
0148-0227/85/005C-0435$05.00

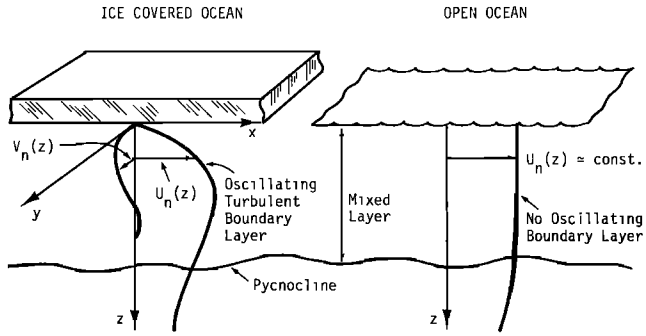

Fig. 1. Schematic illustrating the difference in internal wave boundary conditions between an ice-covered ocean and an ice-free ocean. The boundary layer coordinate system is also illustrated.

eddy coefficient form developed by *Businger and Arya* [1974]. Our philosophy in using the model is to obtain a conservative but realistic estimate of the dissipation, not to explore the nuances of how internal waves interact with each other and the mean flow. For this reason, the nonlinear interactions of the waves in the boundary layer are ignored. We assume that the velocity scale and magnitude of the eddy coefficient are determined by the mean flow and are independent of the internal wave field. This linear model is relatively easy to interpret and yields dissipation values which should be conservative. The underice energy dissipation will be compared with dissipation estimates for the open ocean, and the effect on the internal wave energy in the Arctic will be assessed.

2. The Dissipation Model

From *Long* [1981] the governing equations for the boundary layer motion under the ice are

$$\frac{\partial U}{\partial t} - fV = -\frac{1}{\rho}\frac{\partial p}{\partial x} + \frac{\partial \tau_x}{\partial z} \tag{1}$$

and

$$\frac{\partial V}{\partial t} + fU = -\frac{1}{\rho}\frac{\partial p}{\partial y} + \frac{\partial \tau_y}{\partial z} \tag{2}$$

where U and V are the mean horizontal velocity components in the x and y directions, respectively; z is positive down (see Figure 1); t is time; ρ is density; $\partial p/\partial x$ and $\partial p/\partial y$ are the pressure gradients driving the boundary layer flow; and τ_x and τ_y are the Reynolds velocity correlations $-\overline{u'w'}$ and $-\overline{v'w'}$, respectively. Because z is defined here as positive downward, rotation in the cyclonic sense is negative, and the Coriolis parameter f is taken as -0.0833 cph. In solving the boundary layer problem the depth range is from the roughness scale z_0 at the top to outside the boundary layer $z \to \infty$, at the bottom. In practice, z_0 is a few centimeters while $z \to \infty$ corresponds to about 50 m.

Equations (1) and (2) can be posed in the complex horizontal plane by first defining $C = U + iV$, $\nabla_h = (\partial/\partial x) + i(\partial/\partial y)$, and $\tau = \tau_x + i\tau_y$ and replacing the pressure gradient terms with the time-dependent velocity C_∞ just outside the boundary layer:

$$-\frac{1}{\rho}\nabla_h p = \frac{\partial C_\infty}{\partial t} + ifC_\infty \tag{3}$$

Then (1) and (2) can be written as

$$\frac{\partial}{\partial t}(C - C_\infty) + if(C - C_\infty) = \frac{\partial \tau}{\partial z} \tag{4}$$

The boundary conditions are

$$C = C_{ice} = U_{ice} + i0 \quad \text{at} \quad z = z_0 \tag{5}$$

and

$$C = C_\infty \quad \text{as} \quad z \to \infty \tag{6}$$

Forcing for the boundary layer motion is established by specifying U_{ice} and C_∞. It is assumed that the velocity field can be decomposed into M rotary components

$$C(z) = \sum_{n=0}^{M} C_n(z) = \sum_{n=0}^{M} D_n(z)e^{i\omega_n t}$$
$$= \sum_{n=0}^{M} [A_n(z) + iB_n(z)]e^{i\omega_n t} \tag{7}$$

and

$$C_\infty = \sum_{n=0}^{M} D_{\infty n}e^{i\omega_n t} \tag{8}$$

The motion includes a steady component $n = 0$, corresponding to the mean ice velocity relative to the water. Rotary components are chosen as the rms velocity over narrow bands of a GM-type velocity spectrum. In this way the continuous spectrum is represented as a multiline discrete spectrum with the same total energy.

Even though the velocity for an individual wave component varies in the horizontal, the average energy in a frequency band is assumed invariant in the horizontal. The model results are not affected by the assumption of horizontal homogeneity as long as the oscillating boundary layer thicknesses are small compared to the horizontal wavelengths of the motions.

The key step in solving this boundary layer problem is selecting a closure scheme. *Long* [1981] uses an eddy coefficient closure

$$\tau = K\frac{\partial C}{\partial z} \tag{9}$$

where K is of the form

$$K = ku_* ze^{-6|\omega + f|z/u_*} \tag{10}$$

and $k(= 0.41)$ is von Karman's constant, u_* is a characteristic friction velocity, and ω is the driving frequency. The model has been tested satisfactorily by *Long* [1981] against laboratory experiments for constant density flows driven at a single frequency by rotating or oscillating barotropic pressure gradients or boundary stresses. Under steady flow conditions the model reduces to that of *Businger and Arya* [1974]. In the time-dependent flows the eddy coefficient is independent of time.

The latter feature is of particular interest here. *Long* [1981] found experimental evidence that the constant K works for the purely oscillatory flow case. That is a rather extreme test of the temporal stability of the momentum-transferring properties of the turbulence because the turbulent kinetic energy production term $\tau(\partial C/\partial z)$ varies dramatically in time (as $\cos^2 \omega t$). This implies that the residence time of the turbulent conditions is long compared to the driving period. Hence the effect of turbulence can be scaled quite satisfactorily with the integral flow properties.

Finally, a determination must be made of the appropriate integral scales with which to characterize K for flows with multiple frequency components. This is difficult in principle because the components interact nonlinearly owing to bound-

ary layer turbulence. In practice the lower limit on K can be estimated by assuming that the momentum-transferring properties of the turbulence field are due only to the most persistent flow component, i.e., the steady component due to the ice motion. For this case the scale friction velocity u_* is that due to the stress, which would exist if only the steady motion were occurring. So, $u_* = u_{*\text{ice}} = |\tau_0|^{1/2}$ and

$$K = k u_{*\text{ice}} z e^{-6|f|z/u_{*\text{ice}}} \tag{11}$$

This is reasonable when the steady flow is very much larger than the oscillating components. It represents a minimum value of K (and results in conservative estimates of dissipation) because the addition of oscillating velocity components would increase the level of turbulence and the dissipation rate at all depths.

With this K the solution is of the form given in (7). The complex velocity $D_0(z)$ is the ice motion component. It satisfies the ice motion boundary condition at z_0 and decays to zero as $z \to \infty$. Hence

$$if D_0 = \frac{\partial}{\partial z} K \frac{\partial D_0}{\partial z} \qquad \begin{matrix} D_0 = U_{\text{ice}} & \text{at} & z = z_0 \\ D_0 = 0 & \text{as} & z \to \infty \end{matrix} \tag{12}$$

The wave motion components are $D_n(z)e^{i\omega_n t}$, and each satisfies

$$i(\omega_n + f)(D_n - D_{\infty_n}) = \frac{\partial}{\partial z} K \frac{\partial D_n}{\partial z} \qquad \begin{matrix} D_n = 0 & \text{at} & z = z_0 \\ D_n = D_{\infty_n} & \text{as} & z \to \infty \end{matrix} \tag{13}$$

The dissipation $Q(z, t)$ is given as the energy sink term in the (ensemble) mean kinetic energy equation and appears as shear production in the turbulent kinetic energy equation

$$\begin{aligned} Q(z, t) &= \tau \frac{\partial C'}{\partial z} \\ &= K \frac{\partial C}{\partial z} \frac{\partial C'}{\partial z} \\ &= K\left[\left(\frac{\partial U}{\partial z}\right)^2 + \left(\frac{\partial V}{\partial z}\right)^2\right] \end{aligned} \tag{14}$$

where prime (') denotes complex conjugate. Using (7) in (14) and computing the time average $\bar{Q}(z)$ of $Q(z, t)$ yields

$$\bar{Q}(z) = K \sum_{n=0}^{M} \left[\left(\frac{\partial A_n}{\partial z}\right)^2 + \left(\frac{\partial B_n}{\partial z}\right)^2\right] \tag{15}$$

This gives the mean energy dissipation per time per unit mass at each level in the flow. When multiplied by ρ, it gives the rate of energy loss per unit volume as a function of z. The total energy loss for the water column is found by integrating (15) with respect to z over the whole water column, i.e.,

$$\langle \bar{Q} \rangle = \int_{z_0}^{\infty} \rho K \sum_{n=0}^{M} \left[\left(\frac{\partial A_n}{\partial z}\right)^2 + \left(\frac{\partial B_n}{\partial z}\right)^2\right] dz \tag{16}$$

The final calculation gives the energy lost from the wave field alone. Equations (15) and (16) are linear sums of the component contributions to the dissipation. (It works this way because K is assumed constant in time.) Thus the internal wave contribution is only the sum associated with the wave components.

Hence

$$\bar{Q}_{\text{wave}} = \rho K \sum_{n=1}^{M} \left[\left(\frac{\partial A_n}{\partial z}\right)^2 + \left(\frac{\partial B_n}{\partial z}\right)^2\right] \tag{17}$$

and

$$\langle \bar{Q} \rangle_{\text{wave}} = \int_{z_0}^{\infty} \rho K \sum_{n=1}^{M} \left[\left(\frac{\partial A_n}{\partial z}\right)^2 + \left(\frac{\partial B_n}{\partial z}\right)^2\right] dz \tag{18}$$

The system is solved by specifying z_0, f, U_{ice}, and a series of M frequencies ω_n and velocities $A_{\infty n}$ that characterize the wave field. For convenience, it is assumed that $B_{\infty n} = 0$, since the phase does not affect the dissipation estimates. Equations (12) and (13) are then solved numerically using K from (11).

In the numerical scheme the stress equations corresponding to (12) are actually integrated by assuming an initial estimate of $u_{*\text{ice}}$ and using (11). The resulting surface velocity, determined by integrating the stress equation, is compared with U_{ice}, and an improved estimate of $u_{*\text{ice}}$ is made. This process is iterated until the estimates converge. The solution for the wave components is similar, but it is not necessary to change the value of K derived in solving (12).

3. Forcing and Model Parameters

To apply the model, steady and internal wave velocity components must be specified. The steady component is the mean ice motion. For most runs we have assumed a value of 7 cm s^{-1}, which corresponds to the rms ice velocity measured in the Arctic Basin with drifting ARGOS buoys (R. Colony, personal communication, 1982).

The internal wave velocity components are derived from observations of vertical displacement at 50–150 m depth at the Fram III ice camp [*Levine et al.*, 1985]. The *Desaubies* [1976] formulations of the GM spectra,

$$S_\zeta(\omega) = \frac{2f}{\pi N} r\omega^{-2}(1 - f^2/\omega^2)^{1/2} \tag{19}$$

$$S_u(\pm\omega) = 4\pi r f N \frac{(\omega + f)^2}{\omega^3(\omega^2 \pm f^2)^{1/2}} \tag{20}$$

were used to parameterize the data. A local Brunt-Vaisala frequencey N of 3 cph and a value of the energy parameter r of 50 cm^2 cph were found to be representative of the data. These values were used in (20) to determine the internal wave velocity spectra shown in Figure 2. The velocity which drives the boundary layer motion is that at the very base of the mixed layer, at the outermost edge of the boundary layer. The velocity just below the mixed layer, as represented by the spectra of Figure 2, provides a conservative estimate of this driving velocity because the internal wave velocity mode shapes approach a maximum magnitude going from the pycnocline up into the mixed layer. The usual WKB, N scaling does not apply when going from the seasonal pycnocline into the mixed layer.

The spectra of Figure 2 have been divided into spectral bands. At high frequencies the bands are evenly spaced in log of frequency, but their widths decrease at low frequencies in order to resolve the effect of the singularity in the clockwise rotary spectrum at the inertial frequency. The center frequency and equivalent velocity for each band are given in Table 1. The equivalent velocity is the rms velocity in each frequency band of the clockwise (+) and anticlockwise (−) rotary components. In this way the spectra are represented as single rotary components at the center frequencies.

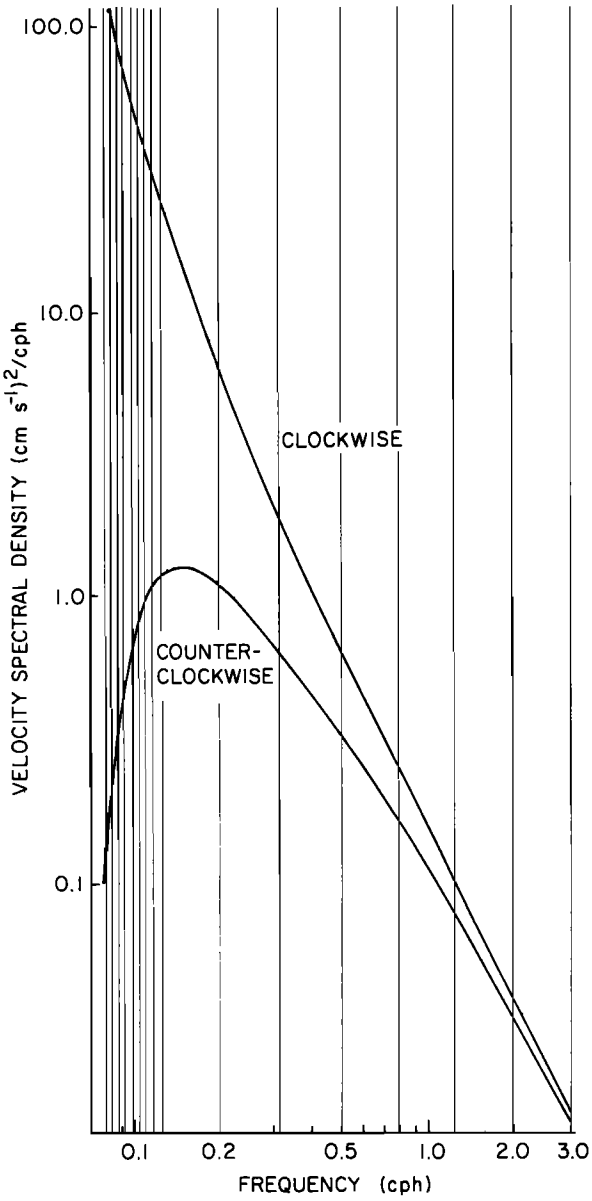

Fig. 2. The internal wave velocity rotary spectra used for input to the boundary layer model. The total energies in the vertical bands are computed and assumed to apply at the band center frequencies.

The one additional parameter necessary to solve the boundary layer problem is z_0. Estimated values of z_0 under the Arctic ice range over several orders of magnitude. M. G. McPhee (personal communication, 1977) statistically analyzed ice force balances during summer conditions to determine a drag law for ice moving over water:

$$\bar{\tau} = C_w \rho \bar{V}_i |\bar{V}_i| e^{i\beta} \tag{21}$$

where $\bar{V}_i$ is the complex ice velocity ($V_{\text{east}} + iV_{\text{north}}$), $C_w = 0.0055$, and $\beta = 23°$. This is the drag law used in the Arctic Ice Dynamics Joint Experiment (AIDJEX) model [*Pritchard*, 1980]. Our model for the steady case was run for varying values of z_0 until, for $z_0 = 3.4$ cm, C_w equal to 0.0055 was obtained. For this value of z_0 the model produced a β of 24°, close to McPhee's statistically derived value of β.

4. Simulation Results

Simulations were run using the forcing and parameters just described. Figure 3 shows $K(z)$ for $u_{\text{ice}} = 7.0$ cm s^{-1} and $z_0 = 3.4$ cm. The linear increase near the surface and the exponential decrease at greater depth result in a maximum $K(z) = 46.4$ cm^2 s^{-1} at 6 m depth.

Figure 4 shows the shape of velocity profiles for several rotary components. They are solutions of (13) normalized by the freestream velocity $A_{n\infty}$ or, in the case of the ice motion component, by the imposed ice velocity. The boundary layer thickness for an oscillating boundary layer scales as $|\tau_n|^{1/2}|\omega_n + f|^{-1}$, where τ_n is the nth component of surface stress and ω_n is the frequency. Thus the boundary layer is thin for large negative frequencies and reaches a maximum thickness for frequencies close to $-f$ (0.0833 cph) such as $\omega = 0.0842$ cph. The model constrains the velocity to reach the freestream value at 50 m and thus imposes a limit on boundary layer thickness for components very close to minus the inertial frequency. To see if this affected dissipation estimates, the depth where velocities were constrained to reach freestream values was varied from 25 to 100 m. This was found to have an effect on the velocity profiles away from the boundary but not near the boundary. The effect on the dissipation estimates is negligible because dissipation occurs very close to the boundary. For frequencies above 0.0833 cph, boundary layer thickness decreases with increasing frequency.

For frequencies less than 0.0833 cph, velocity hodographs look as they do for a steady boundary layer, i.e., looking downward, velocity veers to the right with increasing depth. At frequencies greater than 0.0833 cph the velocity veers to the left with depth. Similarly, stresses are oriented relative to velocity in the usual manner (with velocity to the right of stress) for frequencies less than 0.0833 cph and in the opposite manner for greater frequencies.

Figure 5 shows the dissipation spectrum for $r = 50$ m^2 cph, $z_0 = 3.4$ cm, and K as in Figure 4. The spectrum was formed by computing the energy dissipation, integrated over depth, for each frequency component and then normalizing by the frequency bandwidth. Clockwise and counterclockwise components were added to form the spectrum. The total dissipation of internal wave energy was computed using (18). As

TABLE 1. Dissipation Model Input Parameters for Rotary Components

Frequency, rad/s	Free Stream Velocity, cm/s	
	Clockwise	Counterclockwise
0.08359	0.825	0.001
0.08422	0.528	0.003
0.08480	0.462	0.004
0.08537	0.421	0.005
0.08594	0.391	0.006
0.08657	0.371	0.007
0.08715	0.354	0.008
0.08778	0.341	0.008
0.09053	0.844	0.035
0.09574	0.711	0.049
0.10118	0.626	0.061
0.10703	0.565	0.070
0.11310	0.515	0.078
0.11958	0.477	0.085
0.12645	0.443	0.091
0.16301	0.967	0.301
0.25502	0.637	0.317
0.39998	0.456	0.295
0.62498	0.338	0.257
0.97901	0.259	0.217
1.53003	0.199	0.177
2.40001	0.156	0.196

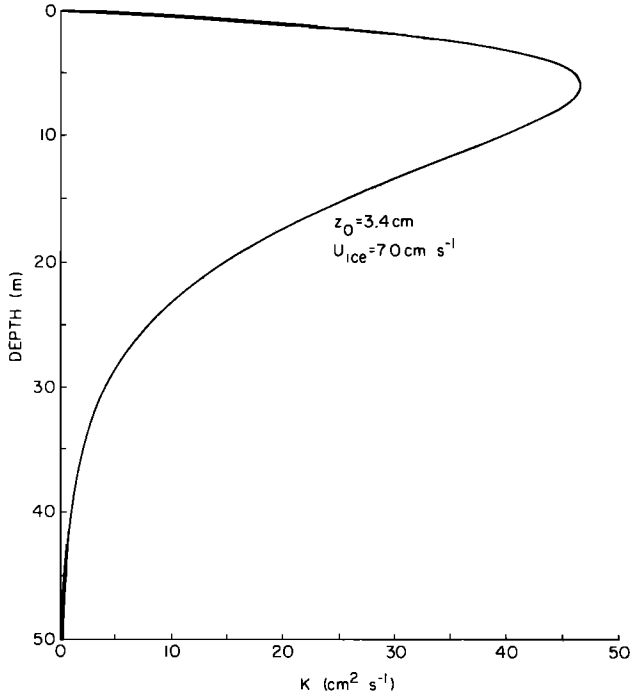

Fig. 3. The model eddy coefficient due to an ice motion of 7.0 cm s^{-1}.

illustrated in Figure 5, the dissipation varies as ω^{-2} just as the internal wave energy does. The reason for this can be seen by performing a scale analysis of the components of (18):

$$\langle \bar{Q} \rangle_{\text{wave component}} \sim \int_{z_0}^{\infty} K \left(\frac{\partial A_n}{\partial z} \right)^2 dz \tag{22}$$

The velocity A_n scales with $A_{n\infty}$, the rms freestream internal wave velocity. As will be shown, dissipation occurs mainly near the surface where the eddy coefficient is proportional to the ice velocity and z:

$$K \sim U_{\text{ice}} z \tag{23}$$

The boundary layer thickness δ_n for a given frequency component scales as the friction velocity for that component and inversely with frequency for frequencies away from $-f$, $\delta_n \sim u_{*n}/\omega_n$. Using (23) and (9), the component friction velocity can be expressed as

$$u_{*n} \sim (\tau_n)^{1/2} \sim \left(K \frac{\partial A_n}{\partial z} \right)^{1/2} \sim (U_{\text{ice}} A_{n\infty})^{1/2}$$

resulting in

$$\delta_n \sim \frac{(U_{\text{ice}} A_{n\infty})^{1/2}}{\omega_n} \tag{24}$$

Thus (22) yields

$$\langle \bar{Q} \rangle_{\text{wave component}} \sim A_{n\infty} \omega_n^{\,2} \int_0^{\delta_n} z \, dz \sim A_{n\infty}^{\,2} U_{\text{ice}}$$

or

$$\langle \bar{Q} \rangle_{\text{wave component}} \sim r \omega_n^{\,-2} U_{\text{ice}} \tag{25}$$

Thus dissipation is proportional to internal wave energy and ice velocity; there is no dependence on frequency other than that due to the ω^{-2} decrease in internal wave energy. *D'Asaro*'s [1982] model produced a different result. Even for a constant wave energy, his results suggest that dissipation should go to zero at high frequencies. This may be because the thickness in his slab model does not decrease with increasing frequency. *D'Asaro*'s [1982] results would require an energy cascade to lower frequencies to supply dissipated energy, while the model presented here does not. Energy is dissipated in each frequency band in proportion to the amount of energy in the band.

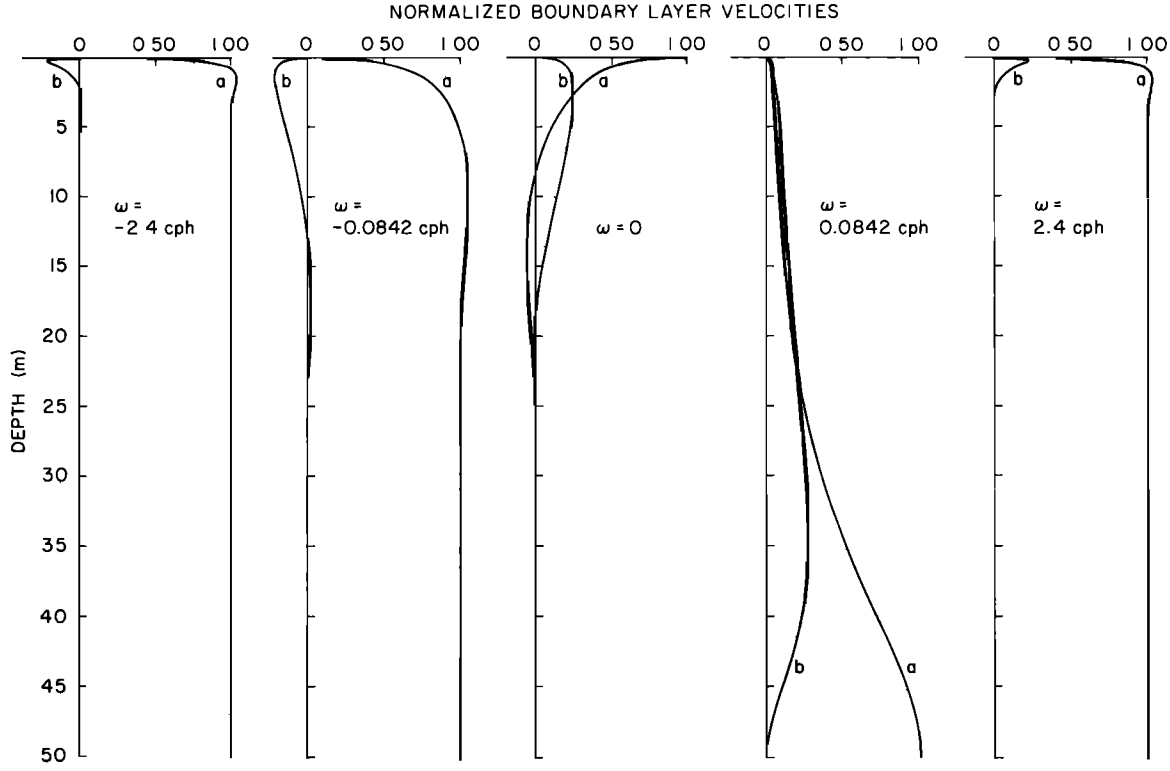

Fig. 4. Boundary layer velocity profiles at five different frequencies, all normalized by the maximum velocity in the profile.

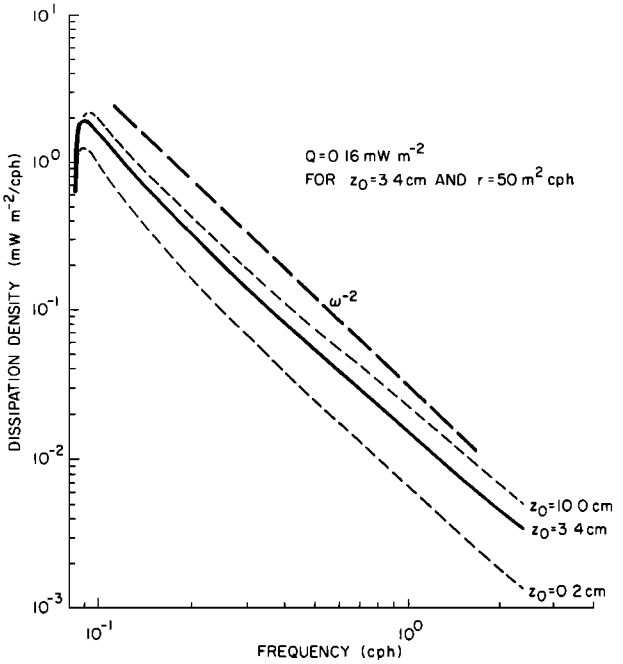

Fig. 5. Dissipation spectra for three different surface roughnesses. The bold dashed line represents an ω^{-2} slope.

The dissipation spectrum decreases at frequencies close to $|f|$ in spite of the singularity in the clockwise velocity spectrum at $w = -f$. This is because the velocity profiles for w_n near $-f$ possess little shear close to the boundary where K is large. In essence, the resonant nature of inertial motion does not allow stress to build up while maintaining a velocity shear adequate to produce dissipation. In nature, the shear for inertial motions occurs at the pycnocline where K is small owing to stratification.

Curves for $z_0 = 10$ cm and $z_0 = 0.2$ cm are also shown in Figure 5. The dissipation spectra for these are within factors of 2 of the values obtained using $z_0 = 3.4$ cm. Thus the results are not critically dependent on surface roughness.

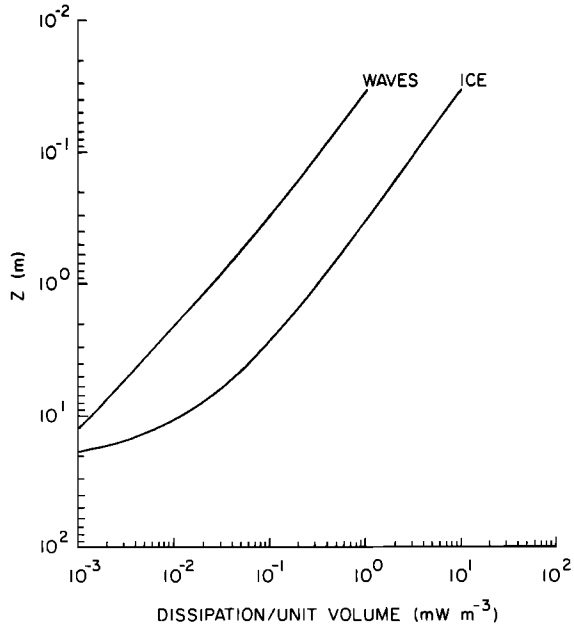

Fig. 6. Dissipation per unit volume plotted versus depth for the wave components and steady ice components.

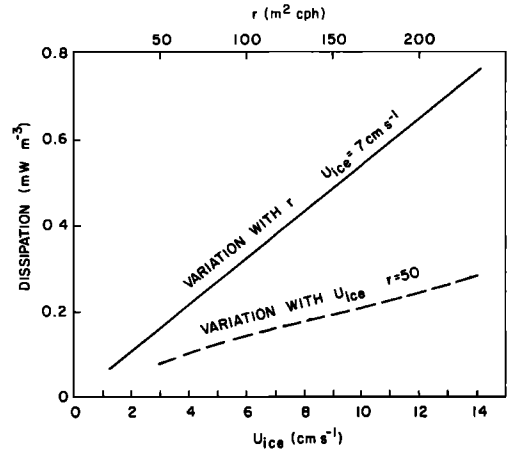

Fig. 7. Total dissipation plotted as a function of r with U_{ice} constant and plotted as a function of U_{ice} with r constant.

In using (23) the assumption is made that the dissipation occurs near the surface. This notion is substantiated by Figure 6, which shows the total dissipation per unit volume for all frequency components as a function of depth. The dissipation for the steady component as a function of depth is also shown. The dissipation per unit volume of internal wave energy drops faster than the inverse of distance from the surface. Over 80% of the dissipation occurs in the top 5 m.

Equation (25) suggests that the total dissipation is linearly related to r and U_{ice}. Figure 7 bears out this relation. It shows the total dissipation as functions of r and U_{ice}. Both variations are approximately linear. On the basis of this result, a simple way to estimate the total dissipation is as the product of an effective internal wave stress $\rho C_{DIS} U_{ice} U_w$ and the internal wave rms velocity U_w. For the results of the model,

$$Q \approx \rho C_{DIS} U_{ice} {U_w}^2$$

and

$$C_{DIS} = 0.0034$$

The dissipation coefficient C_{DIS} is slightly less than the steady state drag coefficient.

5. Discussion

To put these results in perspective, it is useful to compare them with estimates of dissipation from temperate oceans. *Olbers* [1983] lists dissipation estimates based on the work of several authors. In his Table 1, *Olbers* [1983] interprets the measurements of velocity shear microstructure by *Osborn* [1978] as suggesting 1 mW m^{-2} of internal wave energy is dissipated in the upper ocean through the generation of turbulence. He cites the work of *Woods* [1968] and states that 5 mW m^{-2} is dissipated in the upper ocean, presumably by wave-induced shear instability. Finally, he refers to *Garrett* [1979] for a dissipation estimate of between 0.01 and 0.1 mW m^{-2} in the main thermocline. Most of the estimates cited by *Olbers* [1983] for all types of energy flux in internal waves are less than 1 mW m^{-2}. On his Table 1 our value of dissipation, 0.16 mW m^{-2}, would be ranked as significant but not dominant.

The most direct point of comparison with our dissipation estimate is work dealing with downward propagation of energy in temperate oceans and dissipation in the bottom

boundary layer. *Leaman* [1976] used electromagnetic velocity profiler data to determine the polarization of horizontal velocity with depth in the Atlantic. He estimated the downward energy flux to be 0.02–0.4 mW m^{-2} and proposed that this amount of energy was dissipated mainly in the bottom boundary layer. *D'Asaro and Perkins* [1984] estimate the downward flux near the same location to be 0.12 mW m^{-2}. *D'Asaro* [1982] has modeled dissipation in the bottom boundary layer for the same area using a slab model with a linearized quadratic drag law. He estimates that the dissipation is between −0.003 and 0.024 mW m^{-2}. The downward flux measurements of *Leaman* [1976] are of the same order as our dissipation estimates. *D'Asaro*'s [1982] estimate is an order of magnitude smaller than ours.

Such comparisons are somewhat inappropriate because the internal wave energy level in the Arctic is lower than the temperate ocean energy levels to which the other flux and dissipation estimates apply. For example, if the r value were equal to the GM canonical value of 325 m^2 cph, then the dissipation in the underice boundary layer would be 1.0 mW m^{-2}. This is comparable to the largest flux estimates in *Olber*'s [1983] Table 1 and is larger than the vertical flux estimates of *Leaman* [1976] and *D'Asaro and Perkins* [1984].

Another way of looking at this is to compare estimates of dissipation time scale. *D'Asaro* [1982] points out that assuming a total internal wave energy of 4×10^3 J m^{-2} [*Garrett and Munk*, 1979], an energy flux of 0.01 mW m^{-2}, representative of his dissipation estimate, would produce a dissipation time scale of 12 years. He concludes that bottom boundary layer dissipation is unimportant. *McComas and Muller* [1981] cite *Gerrett* [1979] and estimate the time scale for dissipation of internal wave energy by internal wave breaking to be 100 days. By comparison, the time scale for boundary layer dissipation under the ice is short. The total internal wave energy is $\rho \bar{N} H r$, where $\bar{N}$ is the average of N over the ocean depth H and $\bar{N}H = 5$ m s^{-1} in the Arctic [*Morison*, 1985]. For $r = 50$ m^2 cph the total internal wave energy is 436 J m^{-2}. Underice dissipation of 0.16 mW m^{-2} results in a dissipation time scale of 32 days. Thus the underice boundary layer dissipation in the Arctic is as important as any other dissipation mechanism is in temperate oceans. Of course, the other mechanisms that dissipate energy in temperate oceans may also act in the Arctic. The boundary layer process is simply an additional means of dissipation that occurs only in the presence of an ice cover.

Can the added dissipation in the underice boundary layer explain the reduced internal wave energy levels? The Arctic value of $r = 50$ m^2 cph assumed for this study is a factor of 6 less than the GM canonical value and a factor of 4 less than the Internal Wave Experiment (IWEX) value [*Levine et al.*, 1985]. A crude model of the internal wave energy balance, which is compatible with the notion of dissipation time scales, illustrates how such a reduction in energy might result from surface boundary layer dissipation. We assume that the total internal wave energy E can be approximated with a first-order differential equation:

$$\frac{dE}{dt} + \frac{1}{\tau_{\text{diss}}} E + \frac{1}{\tau_{bl}} E = S$$

where τ_{bl} is the time constant for energy dissipation in the surface boundary layer, τ_{diss} is the time constant for dissipation by all other means, and S is the source of internal wave energy. For steady state in the open water case, $\tau_{bl} = \infty$, the energy $E = E_{0w}$ would equal $\tau_{\text{diss}} S$. However, for the same amount of forcing but with the imposition of an ice cover, τ_{bl} is finite, and the energy level $E = E_{ic}$ would be $(\tau_{\text{diss}}{}^{-1} + \tau_{bl}{}^{-1})^{-1} S$. Therefore

$$E_{\text{IC}} = \tau_{bl}(\tau_{bl} + \tau_{\text{diss}})^{-1} E_{0w}$$

and for $\tau_{\text{diss}} = 100$ days [*McComas and Muller*, 1981] and $\tau_{bl} = 32$ days from this study,

$$E_{ic} = 0.24 E_{0w}$$

Such a reduction in energy could explain the lower energy levels in the Arctic. Of course, this is not conclusive because the time scales quoted are only estimates and we do not really know how the internal wave forcing in the Arctic compares with that in temperate oceans. The forcing may very well be lower owing to the absence of surface waves and tidal forcing.

Assuming that boundary layer damping is a dominant mechanism in the Arctic, there are other differences that might be expected in the Arctic internal wave field when compared with open ocean conditions. For example, the internal wave energy flux might be upward (at least during periods with little surface forcing), rather than downward as observed by *Leaman* [1976] and *D'Asaro and Perkins* [1984]. If the reduced energy is due to increased damping, there might be a more rapid decay of internal wave energy after a period of energy input; i.e., the ocean would not "ring" as long as in the open water case. As a result, there may be more temporal variability in the internal wave energy. In fact, internal wave energy estimates from the Arctic do vary by over an order of magnitude [*Morison*, 1985; *Levine et al.*, 1985]. Finally, because boundary dissipation is independent of vertical and horizontal wave number for vertical and horizontal wavelengths greater than the mixed layer thickness, the vertical and horizontal wave number spectra might be different from that observed in open water. There may not be the necessity for an energy transfer from low vertical wave numbers to high vertical wave numbers where dissipation could occur as suggested by *McComas and Muller* [1981].

In summary, we conclude that surface boundary layer turbulence is a significant factor in the dissipation of internal wave energy and may be the cause of the reduced levels of internal wave energy found in the Arctic. Further, dissipation in the underice boundary layer may produce other, as yet unmeasured, changes in the internal wave spectrum of the Arctic.

Acknowledgments. This work was supported by ONR Contracts N00014-79-C-0024 and N00014-80-C-0252 to the University of Washington, ONR Contracts N00014-79-C-0004 and N00014-84-C-0218 to Oregon State University, and DOE Contract DE-AT06-76-EV-71025 to U.S. Army, Waterways Experiment Station, Vicksburg, MS.

REFERENCES

Bernstein, R. L., Observations of currents in the Arctic Ocean, *Tech. Rep. 7*, Lamont-Doherty Geol. Observ. of Columbia Univ., Palisades, N. Y., 1971.

Bernstein, R. L., and K. Hunkins, Inertial currents from a three-dimensional array in the Arctic Ocean (abstract), *Eos Trans. AGU*, *52*(4), 255, 1971.

Businger, J. A., and S. P. S. Arya, Height of the mixed layer in the stably stratified planetary boundary layer, *Adv. Geophys.*, *00*, 73–92, 1974.

D'Asaro, E., Absorption of internal waves by the benthic boundary layer, *J. Phys. Oceanogr.*, *12*(4), 323–336, 1982.

D'Asaro, E., and H. Perkins, A near-inertial internal wave spectrum for the Sargasso Sea in late summer, *J. Phys. Oceanogr.*, *14*(3), 489–505, 1984.

Desaubies, Y. J. F., Analytical representation of internal wave spectra, *J. Phys. Oceanogr.*, *6*, 976–981, 1976.

Garrett, C. J. R., Mixing in the ocean interior, *Dyn. Atmos. Oceans, 3*, 239–265, 1979.

Garrett, C. J. R., and W. H. Munk, Space-time scales of internal waves, *Geophys. Fluid Dyn., 3*, 225–264, 1972.

Garrett, C. J. R., and W. H. Munk, Space-time scales of internal waves: A progress report, *J. Geophys. Res., 80*, 291–297, 1975.

Garrett, C. J. R., and W. H. Munk, Internal waves in the ocean, in *Annu. Rev. Fluid Mech., 11*, 339–369, 1979.

Leaman, K. D., Observations on the vertical polarization and energy flux of near-inertial waves, *J. Phys. Oceanogr., 6*, 894–908, 1976.

Levine, M. D., Internal waves in the ocean: A review, *Rev. Geophys., 21*, 1206–1216, 1983.

Levine, M. D., C. A. Paulson, and J. Morison, Internal waves in the Arctic Ocean: Comparison with lower-latitude observations, *J. Phys. Oceanogr., 15*, 800–809, 1985.

Levkov, N. P., and L. V. Cherkesov, The influence of the ice cover on elements of long waves in a two-layer viscous liquid, *Probl. Arctic Antarctic*, Engl. Transl., 43–44, 139–147, 1974.

Long, C. E., A simple model for time-dependent stably stratified turbulent boundary layers, Ph.D. dissertation, School of Oceanography, Univ. of Washington, Seattle, 1981.

McComas, C. H., and P. Muller, The dynamic balance of internal waves, *J. Phys. Oceanogr., 11*, 970–986, 1981.

Morison, J. H., Internal waves in the Arctic Ocean: A review, in *Geophysics of Sea Ice*, edited by N. Untersteiner, Plenum, New York, in press, 1985.

Munk, W., Internal waves and small scale processes, in *Evolution of Physical Oceanography*, edited by B. Warren and C. Wunch, pp. 264–291, MIT Press, Cambridge, Mass., 1981.

Neshyba, S. J., B. T. Neal, and W. W. Denner, Spectra of internal waves: In situ measurements in a multiple-layered structure, *J. Phys. Oceanogr., 2*, 91–95, 1972.

Olbers, D. J., Models of the oceanic internal wave fields, *Rev. Geophys., 21*(7), 1567–1606, 1983.

Osborn, T. R., Measurements of energy dissipation adjacent to an island, *J. Geophys. Res., 83*(C6), 2939–2958, 1978.

Pritchard, R. S., (Ed.), *Sea Ice Processes and Models*, University of Washington Press, Seattle, 1980.

Woods, J. D., Wave-induced shear instability in the summer thermocline, *J. Fluid Mech., 32*, part 4, 791–800, 1968.

Wunsch, C., Geographical variability of the internal wave field: A search for sources and sinks, *J. Phys. Oceanogr., 6*, 471–485, 1976.

Yearsley, J. R., Internal waves in the Arctic Ocean, M.S. thesis, Mech. Eng. Dept., Univ. of Washington, Seattle, 1966.

M. D. Levine, College of Oceanography, Oregon State University, Corvallis, OR 97330.

C. E. Long, Research Division, Coastal Engineering Research Center, U.S. Army Engineer Waterways Experiment Station, Vicksburg, MS 39180.

J. H. Morison, Polar Science Center, Applied Physics Laboratory, University of Washington, Seattle, WA 98195.

(Received December 18, 1984;
accepted February 15, 1985.)